

Upstream propagation of sea-level signals in fluvio-deltaic environments: time-lags and the dynamics of the fluvial surface

M. Kollegger¹, J. Lorenzo-Trueba¹, A.M. Fernandes², A. Singh³, A. Abeyta⁴

¹Department of Earth and Environmental Studies, Montclair State University, 1 Normal Ave. Montclair, NJ 07043

²Department of Earth and Environmental Sciences, Denison University, 100 West College St. Granville, OH 43023

³Department of Civil, Environmental, and Construction Engineering, University of Central Florida, 12800 Pegasus Dr. Orlando, FL 32816

⁴Department of Mathematics, Physical and Natural Sciences Division, University of New Mexico-Gallup, 705 Gurley Ave. Gallup, NM 87301

Corresponding author: Jorge Lorenzo-Trueba (lorenzotruej@mail.montclair.edu)

Twitter handles:

M. Kollegger @madelinepk1

J. Lorenzo-Trueba @JorgeLT000

A.M. Fernandes @climbing_ripple

A. Singh

A. Abeyta @variolax

Key Points:

- The landward portion of the experimental deltaic profile response to sea-level oscillations is delayed by up to half a period.
- Such a delay in the response is associated with subtle changes in the curvature and relief of the deltaic profile.
- Shifts in curvature and relief can lead to river incision and river terrace formation during sea-level rise.

Abstract

Stratigraphic interpretation generally relies upon the assumption that the fluvio-deltaic surface responds uniformly to sea-level changes; however, recent theoretical work suggests that changes in its relief and concavity can influence the propagation of sea-level information upstream and result in geologically long-lived lags in the system response. We test this theoretical result using measurements from a experimental delta subject to high and low magnitude sea-level oscillations. In both cases, changes in relief and curvature of the fluvio-deltaic profile result in the proximal portion of the profile being out of phase with respect to sea-level cycles, whereas the nearshore regions remain in phase. These results underscore the importance of delayed response to sea-level variations in the upstream portion of river deltas, often resulting in net erosion during sea-level rise and potentially complicating the reconstruction of paleo sea-level from deltaic deposits.

Plain Language Summary

Throughout Earth's history, minor or significant changes in sea level have occurred in tandem with changes in global climate. River deltas, which form when sediment-laden rivers meet the ocean, can be sensitive to changes in sea level. Therefore, the deposits of ancient deltas can be used to piece together information about past changes in sea level. However, recovery of such information can be complicated by the different ways in which deltas adjust to sea-level change. For example, a simplified model suggests that the delta part above sea level will experience erosion when sea-level falls and deposition when sea-level rises. In this work, we show that different delta parts can undergo erosion and deposition simultaneously while sea-level is falling or rising. We used an experimental delta to study how different delta parts respond to changes in "sea level". A key finding is that erosion commonly occurs in upstream parts of the delta during sea-level rise, contradicting traditional models. We therefore recommend caution in reconstructions of sea-level change that rely on erosion in the upstream parts of deltas as an indication of sea-level fall.

1 Introduction

The deposits of river deltas can hold important information about environmental changes in Earth's history, such as variations in sea level, sediment supply, or tectonics (e.g., Paola 2000). Sea-level change is considered to be especially important in influencing erosion and deposition in river deltas; the sedimentary records of ancient deltas have been used to reconstruct local or global variations in sea-level (e.g., Vail et al. 1977; Van Wagoner et al. 1990; Blum and Törnqvist 2000, Porębski and Steel 2006; Catuneanu et al. 2009; Blum et al. 2013). Temporal and spatial variability in how a delta responds to changes in sea level can introduce significant uncertainties into reconstructions of past states (e.g., Kim et al., 2006).

In an idealized cross-section of a delta, the shoreline separates the subaerial fluvio-deltaic surface and subaqueous delta foreset (Figure 1a). Within the broad framework traditionally used for evaluating ancient deltaic deposits, periods of sea-level fall are linked to a seaward shift of depositional facies and a uniform lowering of the fluvial surface elevation (Figure 1b); periods of sea-level rise are linked to a landward shift in depositional facies with enhanced sediment deposition on the fluvial surface (Figure 1c). However, several modeling and experimental studies have shown that periods of sea-level fall are not uniformly erosional and periods of sea-level rise are not uniformly depositional (Heller et al. 2001; Kim et al. 2006; Strong and Paola 2010; Anderson et al. 2019).

Allogenic (external) factors, e.g., climate variability, tectonic uplift, and sea-level changes, work together with autogenic (internal) factors, e.g. river avulsion and lateral migration, to develop patterns of erosion and deposition along the fluvio-deltaic surface (Paola et al. 2009; Hajek and Straub 2017). The interaction of autogenic and allogenic influences can complicate the dynamics presented in Figures 1b and 1c. For instance, during sea-level fall, a high sediment supply relative to the length of the fluvial surface can result in geologically long-lived aggradation of the fluvial surface before it begins to degrade (Figure 1d; Swenson 2000; vanHeijst and Postma 2001; Swenson and Muto 2007). Erosional surfaces, formed during sea-level rise by avulsing channels, can also complicate reconstructions (Sheets et al. 2002; Straub 2009).

In this work, we explore mechanisms by which erosion and deposition co-occur across the fluvio-deltaic surface during variations in sea level. Recent theoretical work highlights the

importance of geometric adjustment of the fluvio-deltaic surface during a cyclical change in sea level (Lorenzo-Trueba et al. 2013; Anderson et al. 2019); alterations in the curvature of the fluvio-deltaic surface and its relief above sea level can result in (a) contemporaneous erosion and deposition during sea-level fall (Figure 1e) and sea-level rise (Figure 1f), and (b) delayed response in the proximal (upstream) deltaic region to sea-level changes. We use data from an experimental delta to evaluate the impact of sea-level oscillations on the dynamics of the fluvial surface.

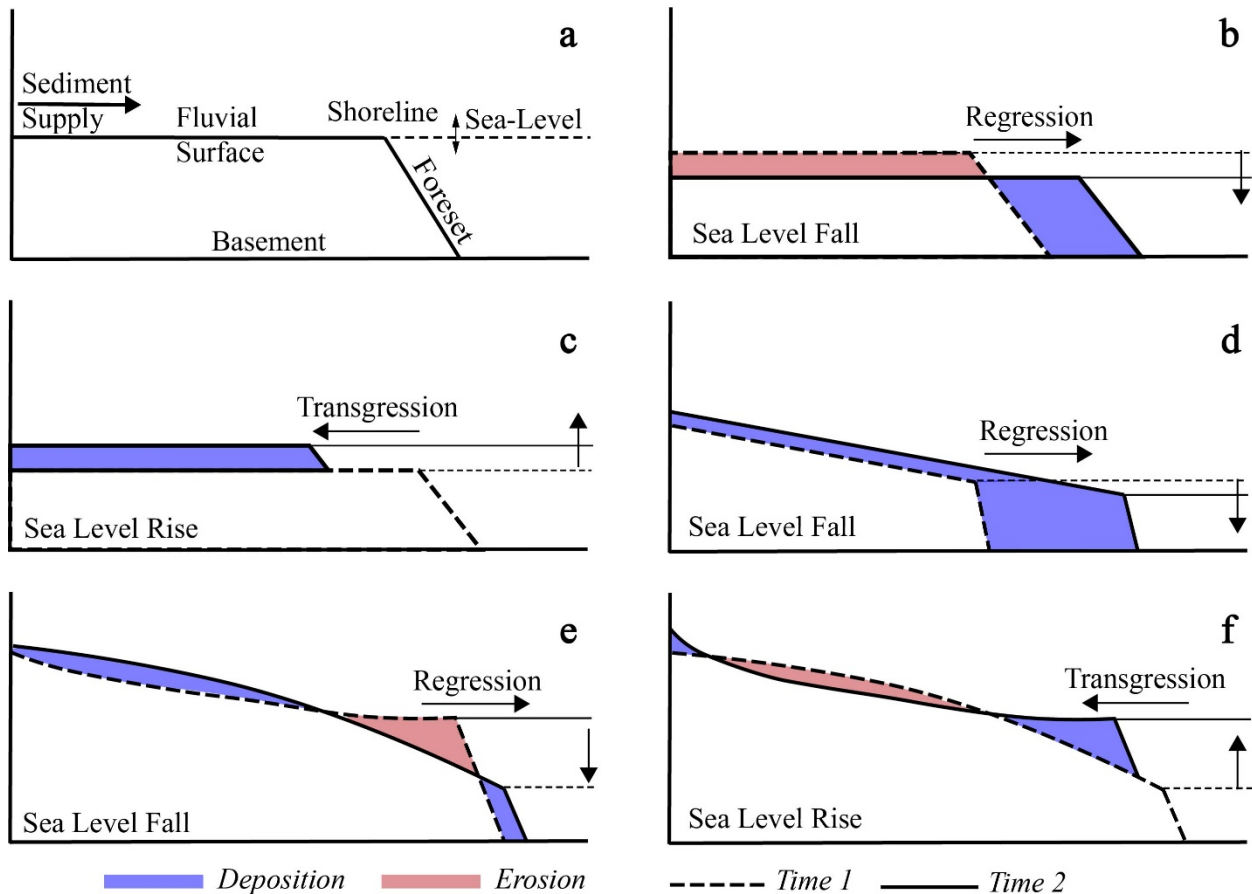
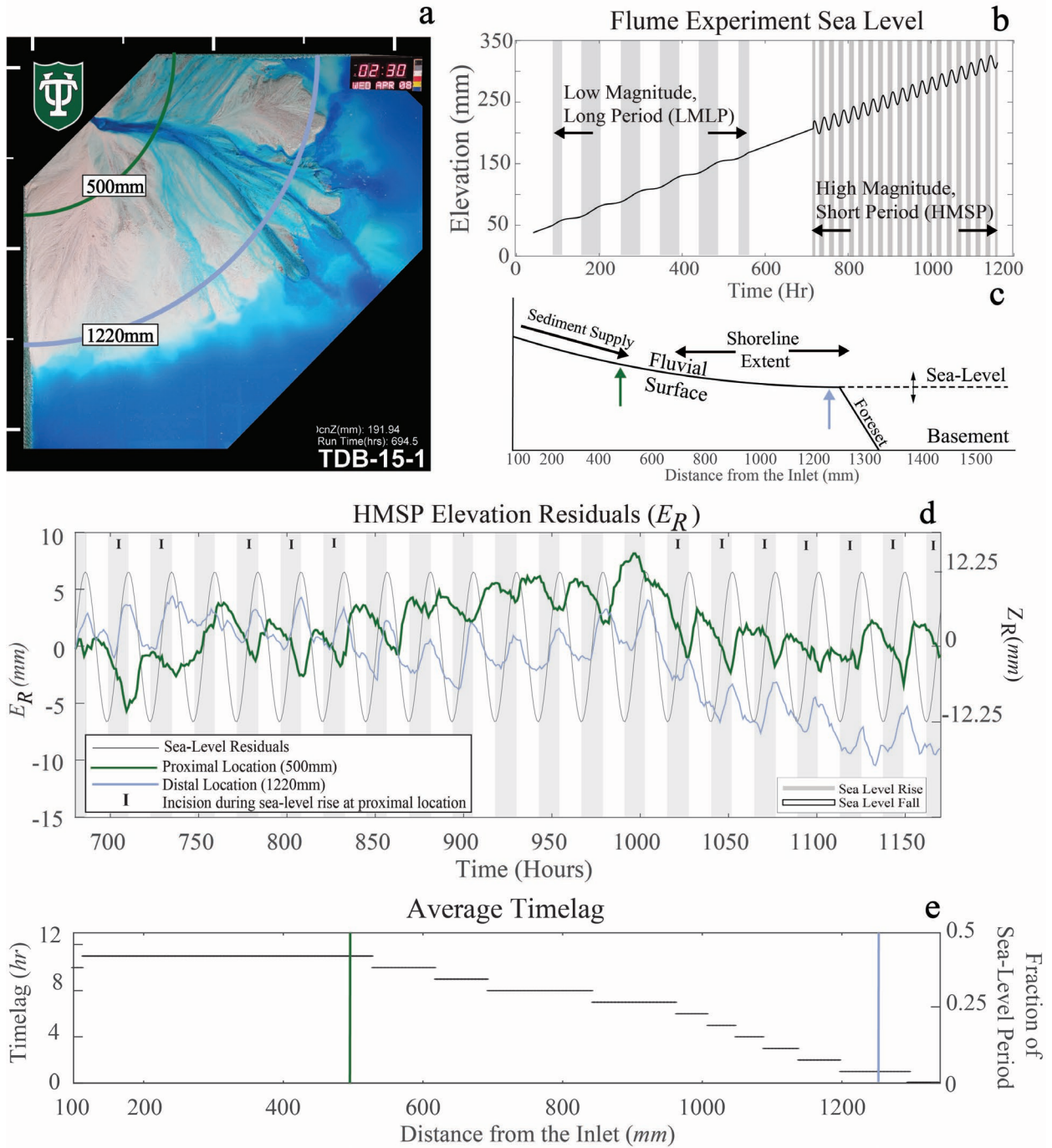


Figure 1. a) Schematic of an ideal longitudinal cross section of a delta, including key processes and domains. b) Negligible fluvial surface slope under sea-level fall. c) Negligible fluvial surface slope under sea-level rise. d) Sloped fluvial surface under sea-level fall. e) Non-linear fluvial surface under sea-level fall. f) Non-linear fluvial surface under sea-level rise.

2 Experimental Conditions and Data Utilized

To quantify the characteristics of longitudinal, up-system propagation of sea-level perturbations and associated dynamics of the fluvial surface, we analyzed an experimental data set from the Tulane Delta Basin (Figure 2a; Li et al. 2016, Yu et al. 2017). In this experiment, a fluvial delta evolved under a constant quartz-dominated sediment supply ($3.9 \times 10^{-4} \text{kg/s}$), constant water input ($1.7 \times 10^{-4} \text{m}^3/\text{s}$), and an imposed sea-level curve depicted in Figure 2b. The sea-level curve

was defined as $Z(t) = Z_B(t) + Z_R(t)$, where $Z_B(t)$ was the background rise in sea-level, assumed to have a constant rate (i.e., $dZ_B/dt = 0.25 \text{ mm/h}$), and $Z_R(t)$ was the "residual" component that included sinusoidal oscillations. Two kinds of oscillations with finite amplitude were superimposed on the background sea-level rise in this experiment: High Magnitude, Short Period (HMSP), characterized by an amplitude of 12.25mm and a period of 24.5 hours, and Low Magnitude, Long Period (LMLP), with an amplitude of 3.06mm and a period of 98 hours. We chose to analyze the fluvio-deltaic surface dynamics in these two scenarios because they represent high and low magnitude forcings relative to the scales of autogenic processes set by channel dynamics. The HMSP and LMLP sections of the experiment ran for 490 hours each and were separated by a shorter period without oscillations (Figure 2b). Overhead photographs (e.g., Figure 2a) were taken every 15 minutes to characterize the flow field, and topographic scans were taken every hour. Given our focus on quantifying the geometric changes of the fluvial surface under the two sea-level scenarios, we primarily analyzed the topographic data (Text S1).



3 Methods Used to Characterize Profile Geometry

To limit the influence of autogenic processes such as channel avulsions on our analysis, we characterize the geometry of the fluvial surface over time t by computing the strike-averaged topographic profile (Figures 2c and S1). We first calculated the radially-averaged elevations $E(x, t)$ at each location x , with $x = 0$ located at the inlet and a step size of 5mm. Coarser resolutions of up to 500mm yielded similar results (Figure S3). Next, we computed the time series of elevation residuals $E_R(x, t)$ by subtracting the background sea-level rise and the reference elevation at $t = t_r$ from the elevation time series (i.e., $E_R(x, t) = E(x, t) - Z_B(t) - E(x, t_r)$; see Figure S2 for additional details). In addition to the average elevations, we also computed the maximum and minimum elevations at different locations along the fluvial surface (Figure S4). We note, however, that average elevations capture changes in the entire fluvial surface, whereas maximum and minimum elevations only represent one location at a given time and for a given distance from the inlet.

We further characterize the profile geometry by defining its relief above sea-level $R(t)$, length $L(t)$, slope $S(t)$, and convexity $\delta(t)$. Both $L(t)$ and $R(t)$ were defined between an upstream location $x_0 = 100 \text{ mm}$, downstream of the inlet to avoid boundary effects, and the shoreline at $x_s = x_0 + L$. Thus, we can express the relief as the difference in elevation between these two locations (i.e., $R = E(x_0, t) - E(x_s, t)$), and the slope $S(t)$ is the ratio between the relief and the length (i.e., $S = R/L$). To compute the convexity metric δ , we first calculate the area difference ΔA between the strike-averaged profile and a linear profile that connects the upstream location at $x = x_0$ and the shoreline location at $x = x_s$ (see Figures 3a and 3b), and then divide it by the length of the profile (i.e., $\delta = \Delta A/L$; see Text S2 for further details on the methodology). In this way, a convex shape to a positive δ value (Figure 3a) and concave corresponds to a negative δ value (Figure 3b).

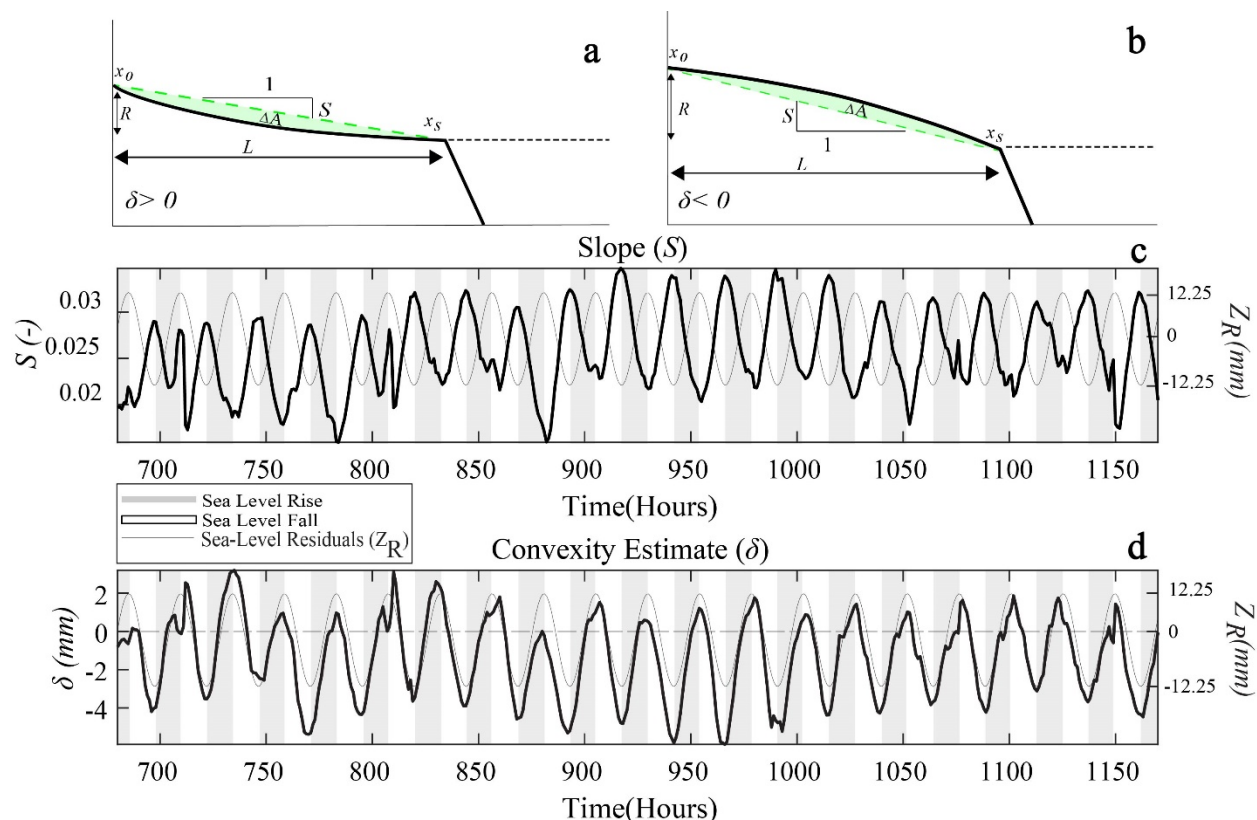


Figure 3. a) Schematic of a convex profile, including the relief R , length L , slope $S=R/L$, and convexity $\delta = \Delta A/L$. The dashed green line represents the idealized linear fluvial surface. b) Schematic of a concave profile. c) Average slope of the fluvial surface through time in the High Magnitude Short Period (HMSP) experimental run. d) Convexity estimate of the fluvial surface through time in the HMSP.

4 The High Magnitude Short Period Scenario

In response to the HMSP sea-level variations, patterns of elevation change were non-uniform across the fluvial surface. Downstream (distal) locations tracked sea-level change. Upstream (proximal) areas reflected sea-level change that occurred roughly half a period earlier, such that elevation residuals increased while sea-level fell and decreased when sea-level rose (Figure 2d). This time lag is noticeable in the minimum elevation time series at the proximal and distal locations; it is also broadly observable, with some variability in the maximum elevation time series (Figure S4). Moreover, we found that the proximal areas often experienced net erosion during the sea-level rise phases (indicated with an "I" in Figure 2d). In contrast, they were net aggradational during sea-level fall in all cases (Figure S2). We quantified this noticeable time lag in the system response by cross-correlating the time series of elevation residuals with the sea-level residuals at every location along the profile (see further details in Text S3). We found that the time lag increased with distance from the shoreline and reached a maximum value of ~ 11 hours, which equals roughly half the period of the sea-level cycles (Figure 2e). We note that the time scale of avulsion, approximately between 10 to 60 hours (Li et al. 2016), generally exceeds the time lag, suggesting that a single lobe is active while the sea-level signal travels upstream. In this case, average elevation changes can be seen as a lower limit of the elevation changes that particularly active specific locations within the fluvial surface can experience. This phenomenon

is illustrated by the higher amplitude of the minimum and maximum elevation time series compared to the average elevation time series (Figure S3).

The average slope and convexity of the fluvial surface also changed as a function of sea level throughout the HMSP experimental run (Figures 3c and 3d). During sea-level rise, the slope S generally decreases, and the convexity metric δ increases; a convex profile is created by a minimum sedimentation rate near the mid-point of the profile (Figure S5). In contrast, during sea-level fall, the maximum sedimentation rate is concentrated near the center of the profile, causing it to shift into a concave shape; this results in a reduction in the convexity metric and an increase in slope. Alternations between a steep and concave profile during sea-level fall and a mild and convex profile during sea-level rise involve sediment transport from proximal to distal locations (Figures 1e and 1f). This subtle process involves vertical changes of just a few millimeters in this experiment. It can explain both the time lag we observe in the response of the proximal region to sea-level variations and the occurrence of river incision occurring during sea-level rise (Figures 2d and S2).

5 LMLP Scenario

Elevation residuals, slope, and curvature associated with the LMLP cycles (Figure 4) show similar, though considerably muted, patterns to those associated with the HMSP cycles. To focus on identifying counterintuitive responses such as river incision during sea-level rise and river aggradation during sea-level fall, we estimate net changes in the profile geometry over the rise and fall sea-level phases.

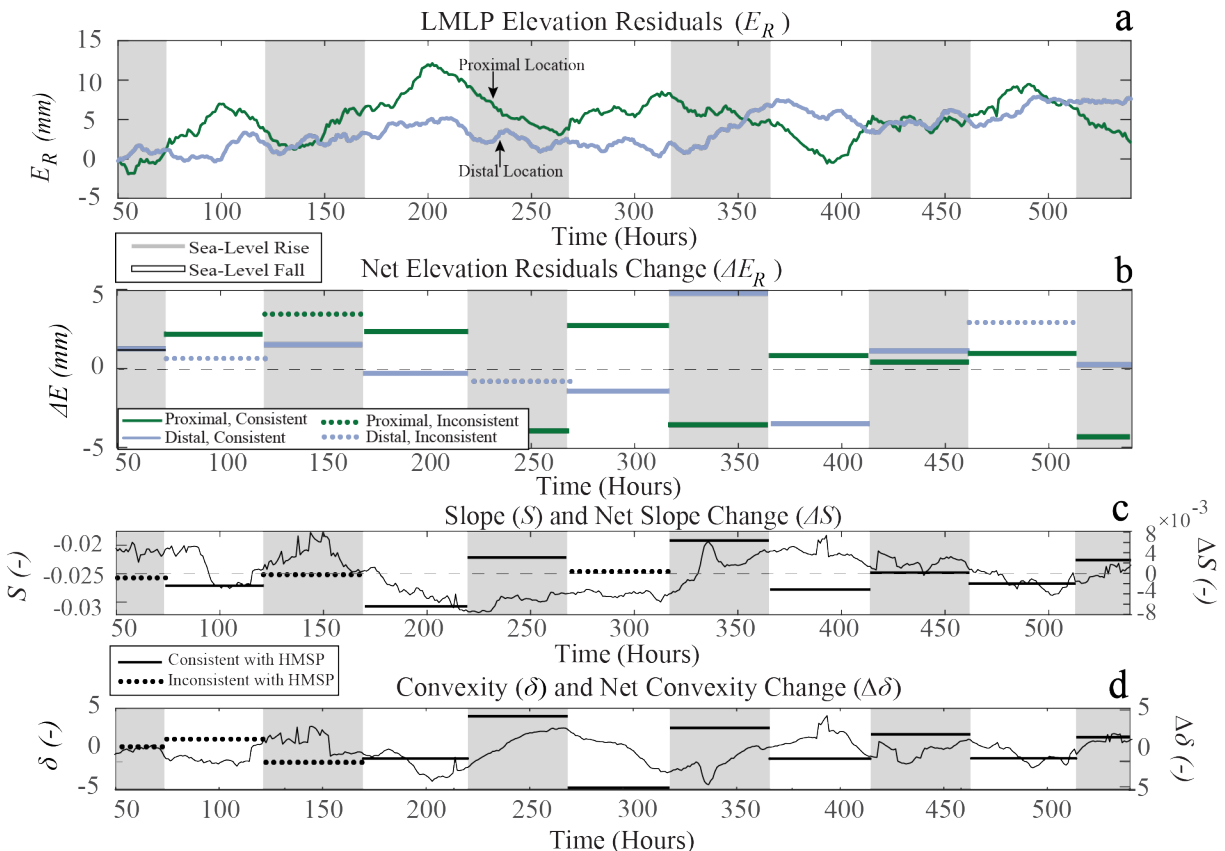


Figure 4. a) Change in residual elevation over time at the proximal and distal locations (Figure 2a) during the Low Magnitude, Long Period (LMLP) experimental run. b) Average residual elevation changes for each sea-level phase. c) Left axis: Slope of the strike averaged fluvial surface through time in the LMLP run. Right axis: Slope change rate in each sea-level phase. d) Left axis: Convexity metric through time in the LMLP run. Right axis: Net change in convexity metric in each sea-level phase. In panels b, c, and d, net changes are in solid line when consistent with the HMSP scenario and dashed line when inconsistent.

During sea-level fall, the elevation of the proximal fluvial surface was more likely to increase, whereas the elevation of the distal regions was more likely to decrease (Figure 4b); conversely, during sea-level rise, elevations of distal areas were more likely to track sea-level and increase, while elevations of proximal regions were more likely to decrease. As in the HMSP case, these results indicate that the proximal delta is mainly expected to be out of phase with respect to sea-level variations (Figure 4a). Changes in average slope (Figure 4d) and convexity (Figure 4f) were similar to those associated with the HMSP cycles; during sea-level rise, the fluvial surface slope decreased and changed into a more convex profile, and the opposite occurred during sea-level fall. These shifts in the geometry of the fluvial surface are due to a change in the spatial pattern of sedimentation (Figure S6); during sea-level rise the spatial pattern is convex with the lowest sedimentation rate located within the proximal region, whereas during the sea-level fall phase the pattern is reversed with a local maximum in sedimentation rate within the proximal region. Consequently, although we do not observe incision at the proximal location as in the HMSP scenario, net sedimentation rates during the sea-level fall are consistently higher than during sea-level rise (Figure S7).

6 Comparisons to Fluvio-deltaic Profiles in Field Settings

Previous sections highlight the key role that changes in fluvial surface geometry play in the response of the experimental delta in the laboratory. In this section, we explore the magnitude of these differences in field settings. To our knowledge, a complete data-set that provides the opportunity to measure slope and concavity of highstand and lowstand fluvio-deltaic profiles from a single system does not exist in the public domain. Therefore, we compare fluvio-deltaic profiles measured in published data from various sources and locations. These data are somewhat incomplete and may not be considered ideal to elucidate the nuanced details of delta dynamics discussed in previous section; however, they do serve to highlight the importance of integrating numerical, experimental and field measurements to understand Earth's rich, complex and incomplete sedimentary record.

We compared the measured slopes of the modern fluvio-deltaic surfaces of the Rio Grande, Colorado, Brazos, Trinity, and Sabine rivers in Texas to the estimated slopes of the fluvio-deltaic surfaces associated with the lowstand deltaic shorelines from 17-22 kya for these systems (Anderson et al. 2016, Text S4, and Table S1). Situated on the Gulf of Mexico shelf margin, these rivers have been subjected to sea-level forcing of a similar magnitude during the last glaciation. We found that at these coarse scales (hundreds of km) the lowstand fluvial profiles of all the rivers measured are steeper than the modern profiles (Table S1). These results are consistent with the experimental data (see Figures 3 and 4) and highlight that the fluvial surface

geometry under sea-level variations is indeed transient. We note, however, that further work is needed to elucidate the relative role of other factors on the dynamics of the fluvial surface, including temporal variations in water and sediment supply and spatial variability in subsidence rates; these factors are not controlled for in the experimental data and could also play a role in field-scale systems.

Working at smaller spatial scales (tens of km) relative to data in Anderson et al. (2016), we used seismic transects (Sylvester et al. 2012, Text S5, and Table S2) to characterize the fluvial surfaces associated with three lobes of the Fuji-Einstein shelf-edge delta, which lies offshore of the modern Mobile River, Alabama. The delta is thought to have been deposited 400-850 kya during a glacial lowstand. At these finer spatial scales, the lowstand fluvial surface is an order of magnitude steeper than the modern highstand fluvial surface of the Mobile River. These high localized slopes at the lowstand delta terminus suggest significant concavity in the shape of the longitudinal profile; substantial changes in the curvature of the fluvio-deltaic surface between highstand and lowstand are more likely to introduce protracted delays in the adjustment of the profile.

Overall, these field examples highlight the contrast in the geometry of the fluvial surface between lowstand and highstand. Such geometric differences in turn reflect the dynamic nature of the fluvial surface and suggest that moderately-sized and large fluvio-deltaic systems (e.g., Colorado, Mississippi) are unlikely to equilibrate to sea-level perturbations at Milankovitch time scales (Hays et al., 1976). Consequently, modern systems that exhibit protracted delays in response to sea-level perturbation are likely to still be in the process of equilibrating to sea-level fall during the last glaciation. In particular, the transition from lowstand to a modern profile involves a decrease in the profile slope and an increase in convexity driven by erosion in proximal locations (despite the rise in sea-level) and sediment deposition in the nearshore; this dynamic is captured by the experiments analyzed herein (Figures 2d and S2). This implies that geomorphic features such as river terraces in proximal locations, conventionally associated with contemporaneous changes in base-level such as relative sea-level fall or uplift (Anderson et al. 2016), could alternatively form during the sea-level rise phase as a result of lengthy equilibration times. For instance, the 14-20 ka Deweyville terrace (Phillips 2006) on the Colorado River formed during sea-level rise after the last glaciation, and its response time has been estimated to be approximately 99 ka (Castelltort et al. 2003). We therefore infer that these adjustments in profile geometry under sea-level variations could have played a role in the formation of river terraces during the Holocene (e.g., Table S3), potentially in combination with other autogenic processes (Hassenruck-Gudipati et al. 2021).

7 Conclusions

We analyzed the propagation of sea-level change information along the fluvial surface of deltaic systems using data from an experimental delta subjected to two types of sea-level oscillations. We found a time lag in response to sea-level change of the proximal fluvio-deltaic surface in both sea-level scenarios. This time lag is introduced by spatially non-uniform adjustments in the relief and convexity of the fluvial surface, such that regions farthest from the shoreline respond with a delay of up to half a period respect to the changes in sea-level. In particular, as the fluvial surface transitions from a steep and concave profile at the end of the sea-level fall phase to a mild and convex shape during sea-level rise, a substantial incision in the proximal delta can

occur. This work implies that river incision and the associated formation of river terraces do not require allogenic forcing such as a fall in relative sea level; thus, we recommend caution when reconstructing contemporaneous uplift or sea-level change rates from river terraces in systems that are prone to protracted delays in response to these changes.

Acknowledgements

This work was supported by NSF-EAR Awards 1854371, 2029803 & 1854452. We thank Elisabeth Steel and Eric Barefoot for their detailed reviews, which helped to improve the quality of the manuscript. We also thank the Tulane Sediment Dynamics and Stratigraphy group for the collection and archival of data. MK would like to thank all members of the MSU Coastal Dynamics Lab for their feedback from the start of this project.

Data Availability Statement

The experimental data used in this paper was accessed at the SEAD Data Repository, project titled *TDB_15_1*. The url is as follows:

<https://sead2.ncsa.illinois.edu/datasets/58dd9ac4e4b0b223acc5ff80>. Access to the database is not restricted, and lies in the public domain.

The codes associated with the data analysis were written in MatLab and can be found on the following Zenodo repository: [DOI: 10.5281/zenodo.5475273](https://doi.org/10.5281/zenodo.5475273). Access to the code is not restricted, and lies in the public domain.

References

Anderson, J. B., Wallace, D. J., Simms, A. R., Rodriguez, A. B., Weight, R. W. R., & Taha, Z. P. (2016). Recycling sediments between source and sink during a eustatic cycle. Systems of late Quaternary northwestern Gulf of Mexico Basin. *Earth-Science Reviews*, 153, 111–138. <https://doi.org/10.1016/j.earscirev.2015.10.014>.

Anderson, W., Lorenzo-Trueba, J., & Voller, V. (2019). A geomorphic enthalpy method: Description and application to the evolution of fluvial-deltas under sea-level cycles. *Computers & Geosciences*, 130, 1–10. <https://doi.org/10.1016/j.cageo.2019.05.006>.

Blum, M.D., & Price, D.M. (1998). Quaternary alluvial plain construction in response to interacting glacio-eustatic and climatic controls, Texas Gulf Coastal Plain. *Shanley, K.W., McCabe, P.W. (Eds.), Relative Role of Eustasy, Climate, and Tectonism in Continental Rocks: SEPM Special Publication*, 59, 31–48. <https://doi.org/10.2110/pec.98.59.0031>

Blum, M. D., & Törnqvist, T. E. (2000). Fluvial responses to climate and sea-level change: a review and look forward. *Sedimentology*, 47(s1), 2–48. <https://doi.org/10.1046/j.1365-3091.2000.00008.x>

Blum, M.D., Martin, J., Milliken, K., & Garvin, M. (2013). Paleovalley systems: Insights from Quaternary analogs and experiments. *Earth-Science Reviews*, 116, 128–169. <https://doi.org/10.1016/j.earscirev.2012.09.003>.

Blum, M.D., & Törnqvist, T.E. (2000). Fluvial responses to climate and sea-level change: a review and look forward. *Sedimentology*, 47, 2–48. <https://doi.org/10.1046/j.1365-3091.2000.00008.x>.

Castelltort, S., & Van Den Driessche, J. (2003). How plausible are high-frequency sediment supply-driven cycles in the stratigraphic record? *Sedimentary Geology*, 157, 3–13. [https://doi.org/10.1016/S0037-0738\(03\)00066-6](https://doi.org/10.1016/S0037-0738(03)00066-6).

Catuneanu, O., Abreu, V., Bhattacharya, J.P., Blum, M.D., Dalrymple, R.W., Eriksson, P.G., Fielding, C.R., Fisher, W.L., Galloway, W.E., Gibling, M.R., Giles, K.A., Holbrook, J.M., Jordan, R., Kendall, C.G.S.C., Macurda, B., Martinsen, O.J., Miall, A.D., Neal, J.E., Nummedal, D., Pomar, L., Posamentier, H.W., Pratt, B.R., Sarg, J.F., Shanley, K.W., Steel, R.J., Strasser, A., Tucker, M.E., and Winker, C., (2009) Towards the standardization of sequence stratigraphy. *Earth-Science Reviews*, 92, p. 1-33. <https://doi.org/10.1016/j.earscirev.2008.10.003>

Erturaç, M.K., Şahiner, E., Zabcı, C., Okur, H., Polymeris, G.S., Meriç, N., & İkiel, C.(2019) Fluvial response to rising levels of the Black Sea and to climate changes during the Holocene: Luminescence geochronology of the Sakarya terraces. *The Holocene*, 29, 941–952, <https://doi.org/10.1177/0959683619831428>.

Hajek, E.A., & Straub, K.M. (2017). Autogenic sedimentation in clastic stratigraphy. *Annual review of earth and planetary sciences*, 45, 681–709. <https://doi.org/10.1146/annurev-earth-063016-015935>.

Hassenruck-Gudipati, H. J., Ellis, T. S., Goudge, T. A., and Mohrig, D.: A multi-proxy assessment of terrace formation in the lower Trinity River valley, Texas, *Earth Surf. Dynam. Discuss.* [preprint], <https://doi.org/10.5194/esurf-2021-37>, in review, 2021.

Hays, J.D., Imbrie, J., & Shackleton, N.J. (1976). Variations in Earths Orbit - Pacemaker of Ice Ages. *Science*, 194, 1121-1132. <https://doi.org/10.1126/science.194.4270.1121>.

Heller, P.L., Paola, C., Hwang, I., John, B., and Steel, R., 2001, Geomorphology and sequence stratigraphy due to slow and rapid base-level changes in an experimental subsiding basin (XES 96-1). *AAPG Bulletin*, 85, p. 817-838. <https://doi.org/10.1306/8626CA0F-173B-11D7-8645000102C1865D>

Hölz, S., (2021). Curve Intersect 2 (<https://www.mathworks.com/matlabcentral/fileexchange/8908-curve-intersect-2>), MATLAB Central File Exchange.

Hsieh, M.-L., & Knuepfer, P.L.K. (2001) Middle–late Holocene river terraces in the Erhjen River Basin, southwestern Taiwan—implications of river response to climate change and active tectonic uplift. *Geomorphology*, 38, 337–372, [https://doi.org/10.1016/s0169-555x\(00\)00105-7](https://doi.org/10.1016/s0169-555x(00)00105-7).

Kim, W., Paola, C., Swenson, J.B., and Voller, V.R (2006), Shoreline response to autogenic processes of sediment storage and release in the fluvial system. *Journal of Geophysical Research*, 111, F04013, <https://doi.org/10.1029/2006JF000470>.

Kock, S., Huggenberger, P., Preusser, F., Rentzel, P., & Wetzel, A. (2009) Formation and evolution of the Lower Terrace of the Rhine River in the area of Basel. *Swiss Journal of Geosciences*, 102, 307–321, <https://doi.org/10.1007/s00015-009-1325-1>.

Latrubesse, E.M., & Franzinelli, E. (2005) The late Quaternary evolution of the Negro River, Amazon, Brazil: Implications for island and floodplain formation in large anabranching tropical systems. *Geomorphology*, 70, 372–397, <https://doi.org/10.1016/j.geomorph.2005.02.014>.

Li, Q., Yu, L., & Straub, K.M. (2016). Storage thresholds for relative sea-level signals in the stratigraphic record. *Geology*, 44, 179–182. <https://doi.org/10.1130/G37484.1>.

Lorenzo-Trueba, J., & Voller, V.R. (2010). Analytical and numerical solution of a generalized Stefan problem exhibiting two moving boundaries with application to ocean delta formation. *Journal of Mathematical Analysis and Applications*, 366, 538–549. <https://doi.org/10.1016/j.jmaa.2010.01.008>.

Lorenzo-Trueba, J., Voller, V.R., & Paola, C., (2013). A geometric model for the dynamics of a fluvially dominated deltaic system under base-level change. *Computers & Geosciences*, 53, 39–47. <https://doi.org/10.1016/j.cageo.2012.02.010>.

Paola, C. (2000). Quantitative models of sedimentary basin filling. *Sedimentology*, 47, 121–178. <https://doi.org/10.1046/j.1365-3091.2000.00006.x>.

Personius, S.F. (1993) Age and origin of the fluvial terraces in the central Coast Range, western Oregon. *U.S. Geological Survey Bulletin*, 2038, <https://doi.org/10.3133/b2038>.

Phillips, J. D. (2006). Geomorphic Context, Constraints, and Change in the lower Brazos and Navasota Rivers, Texas. https://www.twdb.texas.gov/publications/reports/contracted_reports/doc/2005483564_Phillips.pdf (accessed June 2021).

Philips, J.D., & Slattery, M.C., (2007). *Geomorphic Processes, Controls, and Transition Zones in the Lower Sabine River*. Retrieved from https://www.twdb.texas.gov/publications/reports/contracted_reports/doc/0600010595_Sabine.pdf

- Porebski, S.J., and Steel, R.J., 2006, Deltas and sea level change. *Journal of Sedimentary Research*, 76, p. 390–403. <https://doi.org/10.2110/jsr.2006.034>

Schielein, P., Schellmann, G., & Lomax, J. (2011) Stratigraphy of Late Quaternary fluvial terraces at the confluence of the Lech and Danube valleys. *E&G Quaternary Science Journal*, 60, 414–424, <https://doi.org/10.3285/eg.60.4.02>.

Sheets, B., Hickson, T.A., & Paola, C. (2002). Assembling the stratigraphic record: depositional patterns and time-scales in an experimental alluvial basin. *Basin Research*, 14, 287–301. <https://doi.org/10.1046/j.1365-2117.2002.00185.x>

Stinchcomb, G.E., Driese, S.G., Nordt, L.C., & Allen, P.M. (2012) A mid to late Holocene history of floodplain and terrace reworking along the middle Delaware River valley, USA. *Geomorphology*, 169-170, 123–141, <https://doi.org/10.1016/j.geomorph.2012.04.018>.

Straub, K.M., Paola, C., Mohrig, D., Wolinsky, M.A., & George, T. (2009). Compensational Stacking of Channelized Sedimentary Deposits. *Journal of Sedimentary Research*, 79, 673–688, <https://doi.org/10.2110/jsr.2009.070>.

Strong, N., & Paola, C. (2010). Valleys that never were: Time surfaces versus stratigraphic surfaces. *Journal of Sedimentary Research*, 80, 4–5. <https://doi.org/10.2110/jsr.2008.059>.

Swenson, J.B. (2005). Fluviodeltaic response to sea-level perturbations: Amplitude and timing of shoreline translation and coastal onlap. *Journal of Geophysical Research*, 110, <https://doi.org/10.1029/2004jf000208>.

Swenson, J.B., & Muto, T. (2007). Response of coastal plain rivers to falling relative sea-level: allogenic controls on the aggradational phase. *Sedimentology*, 54, 207–221. <https://doi.org/10.1111/j.1365-3091.2006.00830.x>.

Swenson, J.B., Voller, V.R., Paola, C., Parker, G., & Marr, J.G. (2000). Fluvio-deltaic sedimentation: A generalized Stefan problem. *European Journal of Applied Mathematics*, 11, 433–452. <https://doi.org/10.1017/S0956792500004198>.

Sylvester, Z., Deptuck, M., Prather, B., Pirmez, C., & O'Byrne, C. (2012) Seismic Stratigraphy of a Shelf-Edge Delta and Linked Submarine Channels in the Northeastern Gulf of Mexico: Application of the Principles of Seismic Geomorphology to Continental-Slope and Base-of-Slope Systems. *Case Studies from Seafloor and Near-Seafloor Analogues*, 31–59, <https://doi.org/10.2110/pec.12.99.0031>.

Van Heijst, M.W.I.M., & Postma, G. (2001). Fluvial response to sea-level changes: a quantitative analogue, experimental approach: Modelling fluvial response to sea-level changes. *Basin Research*, 13, 269–292. <https://doi.org/10.1046/j.1365-2117.2001.00149>.

Wagoner, J. C., R. M. Mitchum, K. M. Campion, & V. D. Rahmanian (1990). Siliciclastic sequence stratigraphy in Well Logs, cores, and outcrops. *American Association of Petroleum Geologist*, <https://doi.org/10.1306/mth7510>.

Yu, L., Li, Q., and Straub, K.M. (2017). Scaling the response of deltas to relative-sea-level cycles by autogenic space and time scales: A laboratory study. *Journal of Sedimentary Research*, 87, 817–837. <https://doi.org/10.2110/jsr.2017.46>.

Supporting Information for

Upstream propagation of sea-level signals in fluvio-deltaic environments: time-lags, and the dynamics of the fluvial surface

Madeline Kollegger¹, Jorge Lorenzo-Trueba¹, Anjali M. Fernandes², Arvind Singh³,
Antoinette Abeyta⁴

¹*Department of Earth and Environmental Studies, Montclair State University, 1 Normal Ave. Montclair, NJ 07043*

²*Department of Earth and Environmental Sciences, Denison University, 100 West College St. Granville, OH 43023*

³*Department of Civil, Environmental, and Construction Engineering, University of Central Florida, 12800 Pegasus Dr. Orlando, FL 32816*

⁴*Department of Mathematics, Physical and Natural Sciences Division, University of New Mexico-Gallup, 705 Gurley Ave. Gallup, NM 87301*

Contents of this file

Text S1 to S5
Figures S1 to S7
Tables S1 to S3

Introduction

This supplementary material includes the following sections:

Text S1: Code description of the codes used to generate Figures 1 to 4 in the manuscript.

Text S2: Details on how to compute the concavity metric.

Text S3: Details on how to compute the time lag.

Text S4: Methods description for modern to Pleistocene fluvial surface geometry comparison. Text S5: Analysis methodology for the Fuji Einstein Shelf Edge data.

Figure S1: Average Profile Examples.

Figure S2: HMSP Elevation and Elevation Residuals Time Series.

Figure S3: Elevation residuals at the proximal and distal locations using different step sizes.

Figure S4: Mean, maximum and minimum elevation residuals at the proximal/distal locations.

Figure S5: HMSP sedimentation pattern during sea-level rise and fall phases.

Figure S6: LMLP sedimentation pattern during sea-level rise and fall phases.

Figure S7: LMLP Elevation Time Series Analysis.

Table S1: Modern versus lowstand slopes for a collection of Gulf Coast rivers.

Table S2: Fuji Einstein shelf edge delta information.

Table S3: Examples list of river terraces formed during the Holocene.

Text S1.

In this section we include the code description of the codes used to generate Figures 1 to 4 in the manuscript.

The first step was to extract the elevation information of the fluvial surface over time for our analysis. We used the script called "**TopoMatrix.m**" to define two 3D matrices with the

fluvial surface elevations over time for each sea-level scenario. The "**LMLP.mat**" matrix for the Low Magnitude, Long Period (LMLP) scenario, and the "**Anew.mat**" matrix for the High Magnitude, Short Period (HMSP) scenario. Note that this script is not required to reproduce the plots included in the manuscript; "Anew.mat" and "LMLP.mat" are also included in the Zenodo code repository. The link to the SEAD repository can be found in the acknowledgments section of the manuscript. For more details on the experiment, see Yu et al. 2017.

After loading the matrices "Anew.map" or "LMLP.mat", we use the following scripts:

- "**RadialAverageMatrixResiduals.m**" to generate figures 2D and 2E (HMSP scenario).
- "**AverageProfile.m**" to generate figures 3C and 3D (HMSP scenario).
- "**LMLPRadialAverageMatrixResiduals.m**" to generate figure 4A (LMLP scenario).
- "**LMLPAverageProfile.m**" to generate figures 4B, 4C, and 4D (LMLP scenario).

With these scripts, we calculate the radial averages between a location 100mm downstream of the inlet (to avoid boundary effects) and the shoreline with a spacing of 5mm. We locate the shoreline using the curve intersect function (Hölz 2021). In some occasions, the shoreline extends beyond the domain covered by the topographic scans (1.3m from the inlet); in this case we fix the shoreline location at $x=1.3\text{m}$ until it retreats again.

The scripts described in this section have been developed by Madeline Kollegger and Jorge Lorenzo-Trueba. They can be accessed at the Zenodo repository or at <https://github.com/JorgeMSU>.

Text S2.

To compute the convexity metric $\delta(t)$, we divide the area difference between the strike-averaged profile and a linear profile $\Delta A(t)$ by the length of the profile $L(t)$, i.e.,

$$\delta(t) = \Delta A(t)/L(t),$$

where

$$\Delta A(t) = \frac{1}{2} \cdot R(t) \cdot L(t) - \int_{x_0}^{x_s} (E(x, t) - E(x_s, t)) \cdot dx.$$

Location $x = x_0$ corresponds to the upstream location, and location $x = x_s$ matches the shoreline. In this way, a convex profile corresponds to a positive δ value and concave to a negative δ value (Figure S2, Figures 3a and 3b).

Text S3.

In this section, we elaborate on how to compute the time lag. We compute the elevation residuals from the elevation time series as illustrated in Figure S2. Then we compute the time lags in the response at each location along the profile by cross-correlating the elevation residuals time series with the sea-level residuals. In other words, we shift the elevation residuals at a given location by a range of lags and calculate the cross-correlation against the sea-level residuals. The resulting time lag for this particular

location is the one that yields the maximum correlation value. We use the matlab cross-correlation function “xcorr” for this computation (see “RadialAverageMatrixResiduals.m” script). As shown in Figure 2d the time lag for the proximal location is noticeable.

Text S4.

We first identify the intersection of the alluvial-bedrock contact with several modern Gulf Coast Rivers (Table S1) using the following USGS map: <https://mrdata.usgs.gov/geology/state/map-us.html#home>. We then compute the slopes of the modern fluvial surfaces by dividing the difference in elevation and the straight line distance between the alluvial-bedrock contact (measured with Google Earth Pro) and to the modern shoreline. We used the locations of the lowstand systems for each river, as presented by Anderson et al 2016 (their Fig. 11), to identify the location and elevation of the lowstand coastline (22ka-17ka) for each system during the last glacial maximum. These shorelines currently coincide with the ~120m (below mean sea level) bathymetric contour. We used their Figure 11, georeferenced in Google Earth Pro, to calculate the fluvial surface slope associated with the lowstand shoreline from the Last Glacial Maximum (LGM). The estimated fluvial surface slope of the lowstand systems is consistently more than twice the slope of the modern fluvial surface. For additional information, please refer to the expanded spreadsheet uploaded with this supplement and associated with data in Table S1.

Text S5.

We used the seismic data and interpretations of delta lobe stratigraphy presented by Sylvester et al., 2012, to estimate the slope of the delta topset (the fluvial surface) associated with the Fuji Einstein shelf edge delta complex located offshore of the Mobile River, Alabama. The Fuji Einstein delta complex is estimated to have been deposited during a glacial lowstand in sea-level that occurred between 400 ky and 850 ky, a period of time that includes Marine Isotope Stages (MIS) 12 to 20 (Sylvester et al, 2012). Vertical distances were converted from two-way travel time using the conversion 58.4 seconds = 50 m (approximately) from well data presented by Sylvester et al, 2012 in their Figure 20.

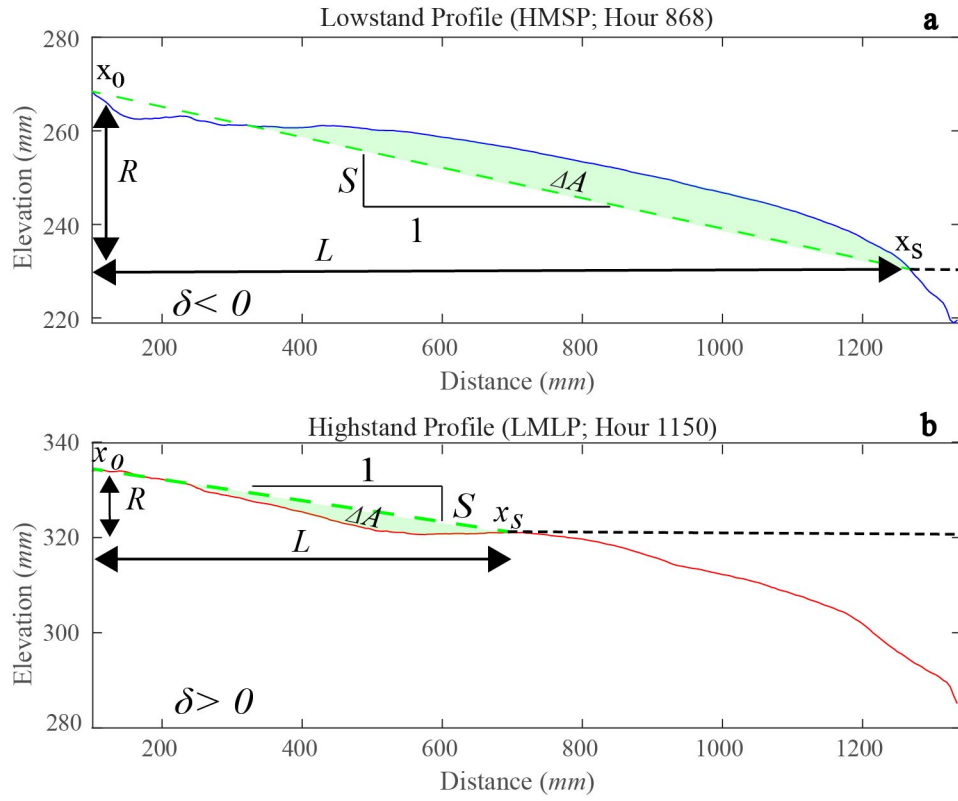


Figure S1. Average Profile Examples.

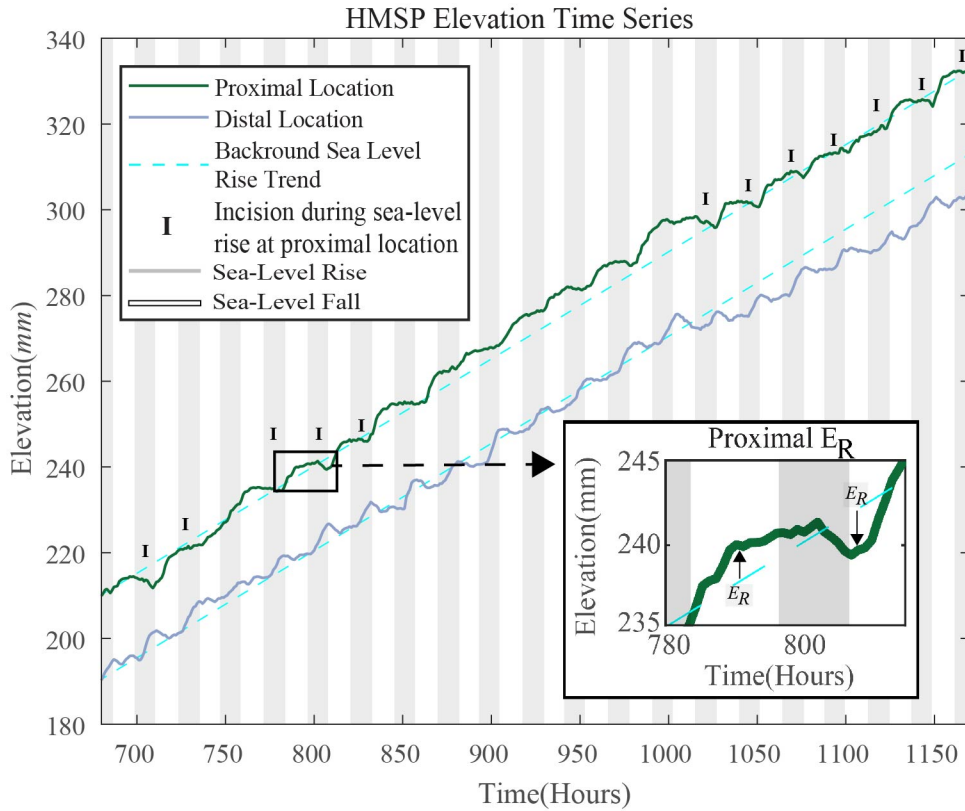


Figure S2. Elevation time series $E(x,t)$ at both the proximal and distal locations for the HMSP scenario. The dashed line represents the background sea-level rise rate (0.25mm/h), and the inset illustrates the relationship the elevation and elevation residuals (E_R).

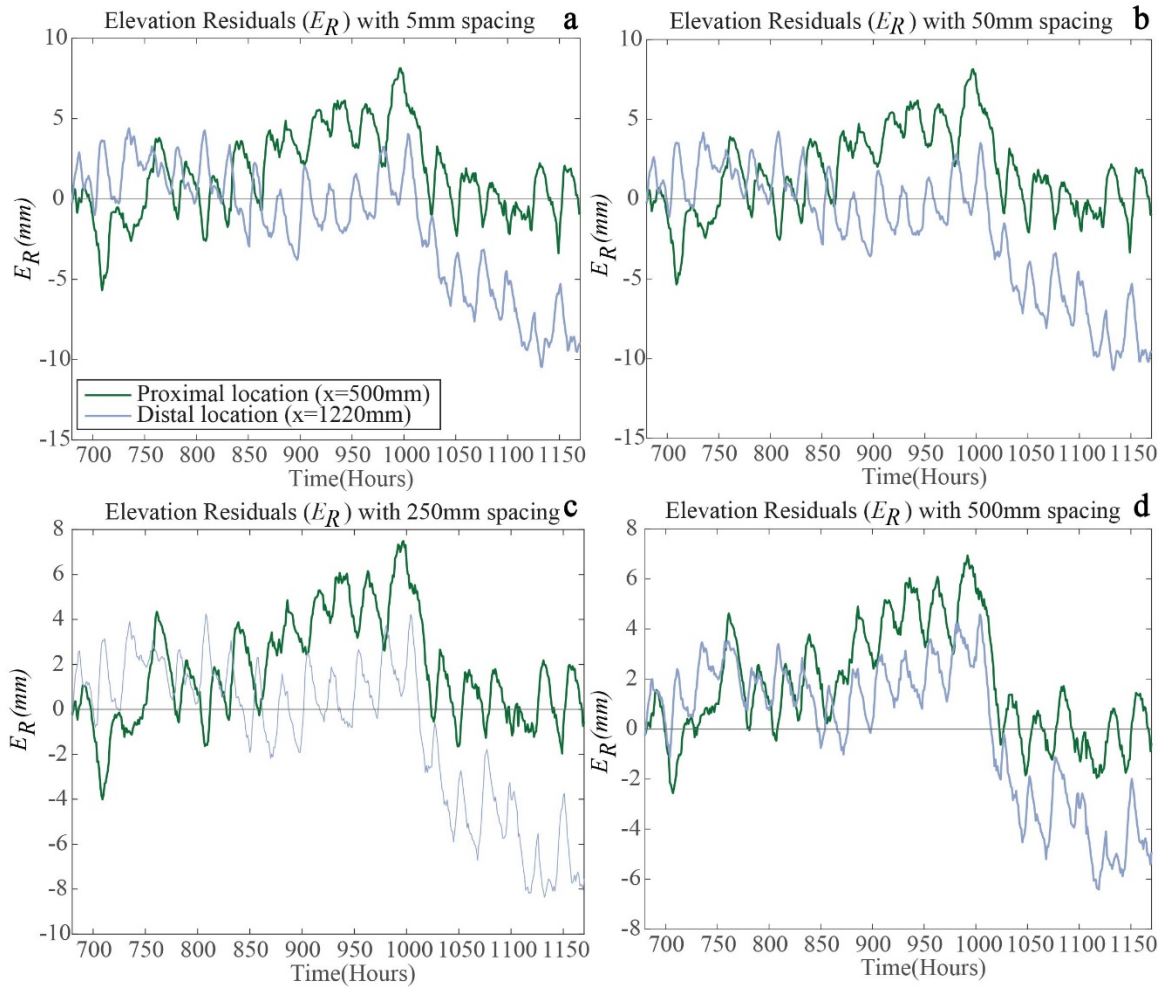


Figure S3. Elevation residuals at the proximal and distal locations using different step sizes: a) 5mm, b) 50mm, c) 250mm, and d) 500mm. Note that the length of the profile is $\sim 1000\text{mm}$. The spatial resolution used to compute the spatial average does not affect the time delay between proximal and distal locations.

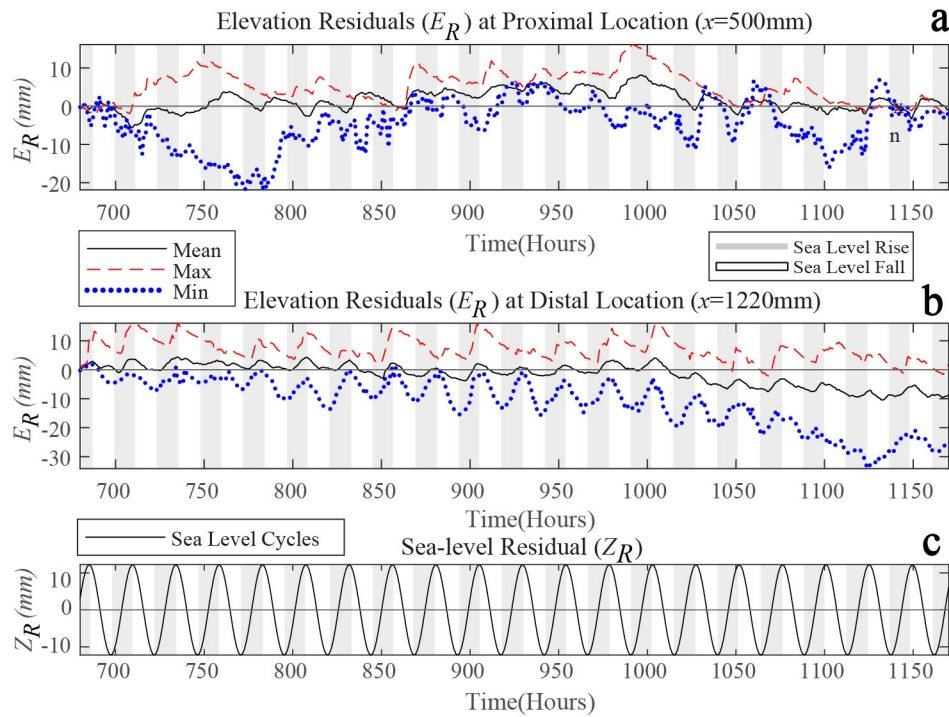


Figure S4. Mean, maximum and minimum elevation residuals at the a) proximal and b) distal locations, with sea-level residuals as a reference in c). Mean, maximum and minimum values are in sync with sea-level changes at the distal location, and out of phase at the proximal location, despite some variability shown by the maximum and minimum elevation residuals. The mean elevation better represents the entire fluvial surface (both active and inactive regions); the maximum and minimum elevations are only representative of specific locations that change with time.

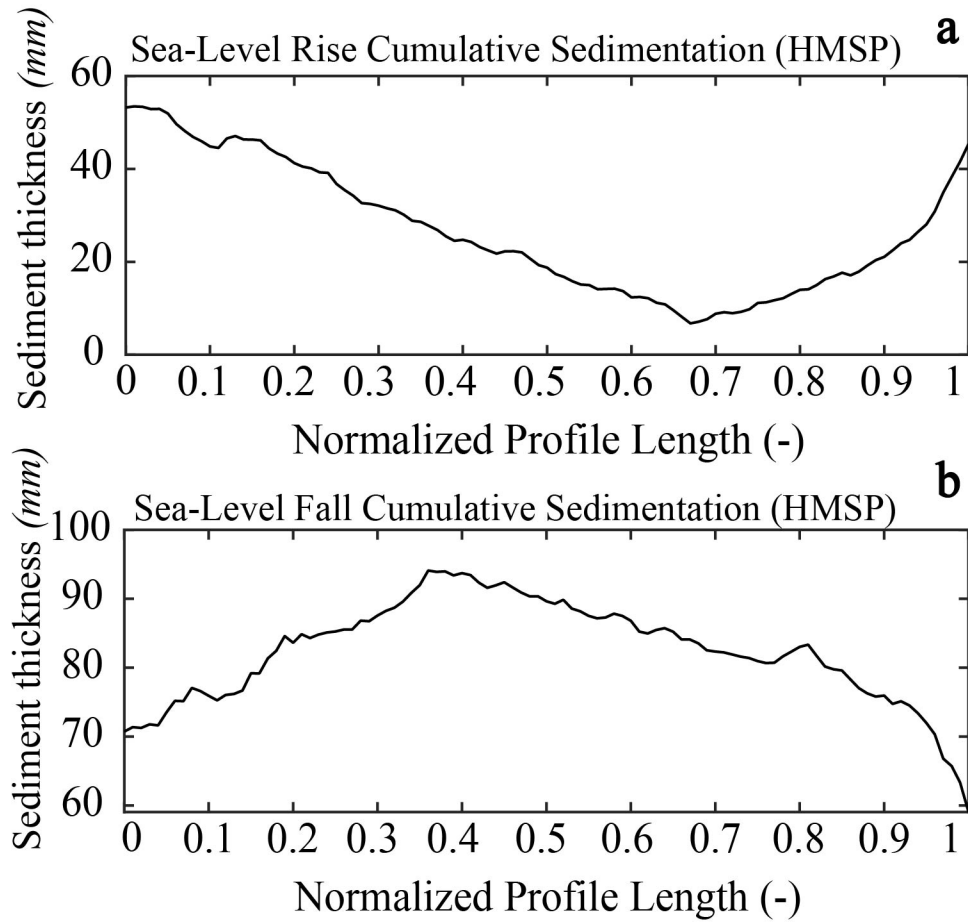


Figure S5. HMSP cumulative sedimentation patterns normalized by profile length over a) sea-level rise and b) sea-level fall phases. The downstream location at $x=1$ matches the shoreline location. Note the shift from a convex pattern during sea-level rise, which enhances the convexity of the profile, to a concave pattern of sedimentation during sea-level fall.

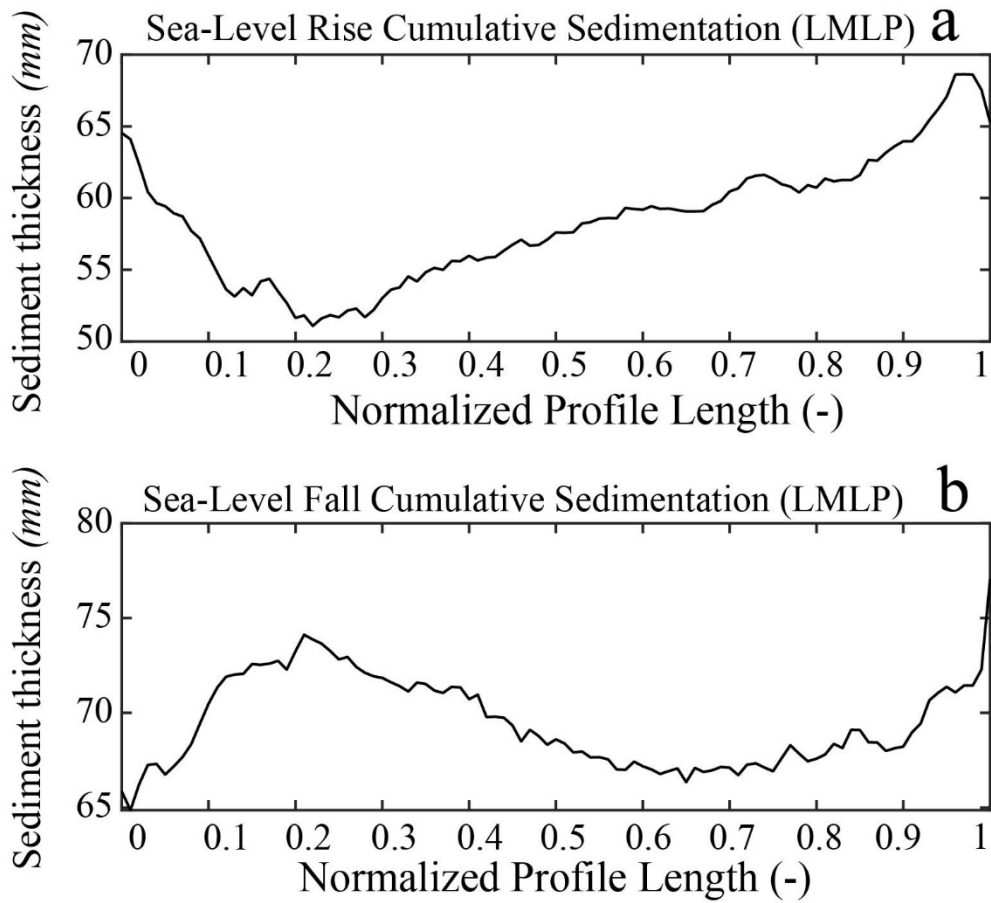


Figure S6. LMLP cumulative sedimentation patterns normalized by profile length over a) sea-level rise and b) sea-level fall phases. The downstream location at $x=1$ matches the shoreline location. Note the shift from a convex pattern during sea-level rise, which enhances the convexity of the profile, to a quasi-concave pattern of sedimentation during sea-level fall.

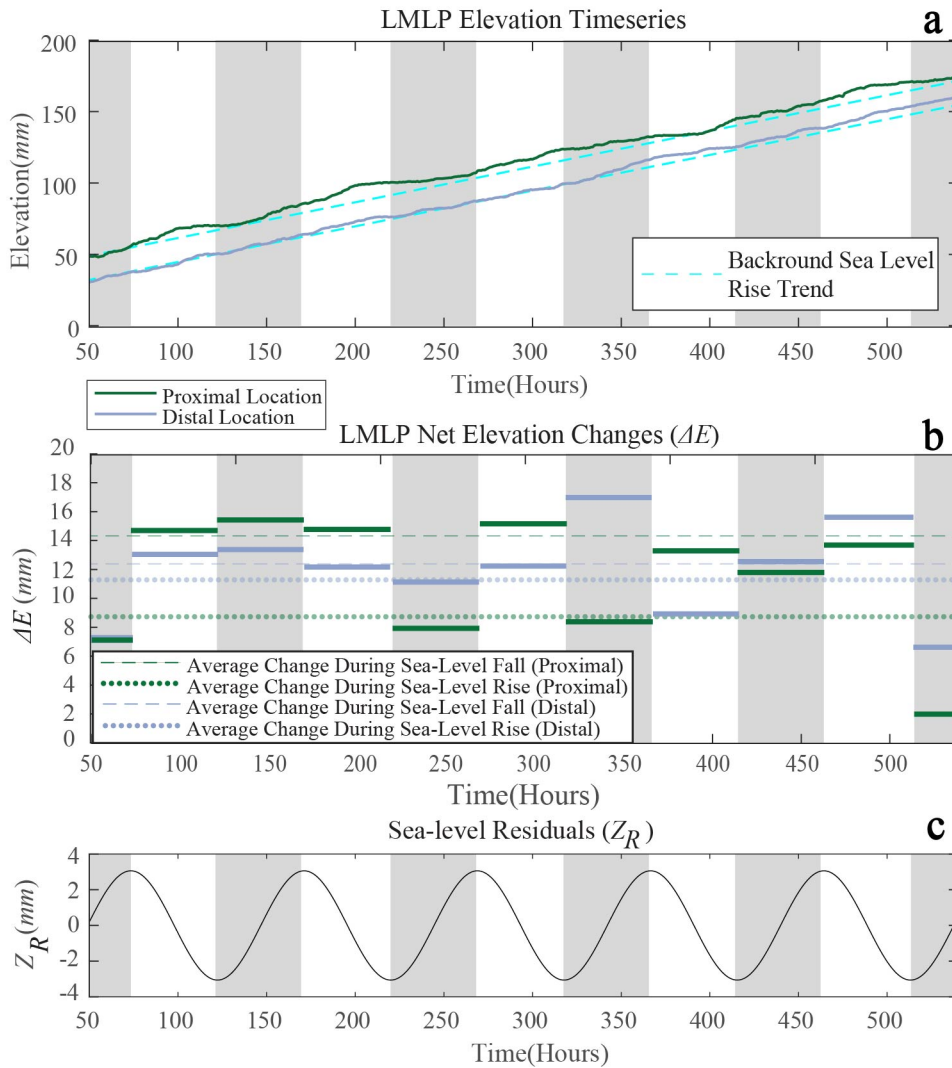


Figure S7. a) Elevation time series $E(x,t)$ at the proximal and distal locations for the LMLP scenario. b) Net elevation change over each sea-level phase at both the proximal and distal locations. At the proximal location, generally higher elevation changes take place during the sea-level rise than during sea-level fall phases. In contrast, net elevation changes at the distal location are similar during sea-level rise and sea-level fall phases. c) Sea-level residuals. Gray bands represent the sea-level rise stages, whereas the white represent sea-level fall.

| River | Modern fluvial surface slope | Lowstand fluvial surface slope |
|--------------------------------------|------------------------------|--------------------------------|
| Rio Grande River, Texas ¹ | -2.7×10^{-4} | -6.7×10^{-4} |
| Colorado River, Texas ¹ | -3.5×10^{-4} | -8.2×10^{-4} |

| | | |
|--------------------------------------|-----------------------|-----------------------|
| Brazos River, Texas ¹ | -2.7×10^{-4} | -6.4×10^{-4} |
| Trinity River, Texas ¹ | -2.7×10^{-4} | -5.1×10^{-4} |
| Sabine River, Texas ¹ | -8.7×10^{-5} | -4.6×10^{-4} |
| * Mobile River, Alabama ² | -1.3×10^{-4} | -3.9×10^{-4} |

Table S1. Modern versus lowstand slopes for a collection of Gulf Coast rivers (Sources: 1- Anderson et al, 2016; 2- Sylvester et al, 2012). *It is unclear how similar the modern Mobile River is to the river that fed the Fuji Einstein delta.

| Delta lobe | Transect 1 | Topset slope | Mean topset slope | Notes |
|------------|------------|------------------------|------------------------|---|
| 5 | Transect 1 | -5.62×10^{-3} | -3.49×10^{-3} | Only lobes with no noted faults were used here. |
| 4 | Transect 1 | -7.66×10^{-3} | | |
| 3 | Transect 1 | -8.06×10^{-3} | | |
| 2 | Transect 1 | -7.39×10^{-3} | | |

Table S2. Delta top-set slope estimated from data digitized from Sylvester et al, 2012, Figure 8.

| River | Terrace | Age (yr) | Deviation (\pm) | Reference |
|-------------|------------------------------|-------------|---------------------|------------------------|
| Delaware | -- | 6000-8000 | -- | Stinchcomb et al. 2012 |
| Lech-Danube | Young Holocene terrace 1.1 | 2350-2730 | -- | Schielein et al. 2011 |
| Lech-Danube | Young Holocene terrace 1.2 | 1600-1900 | 200 | Schielein et al. 2011 |
| Lech-Danube | Young Holocene terrace 2.2.a | 480-650 | -- | Schielein et al. 2011 |
| Lech-Danube | Early Holocene terrace | 10180-11170 | -- | Schielein et al. 2011 |

| | | | | |
|----------------|--------------------------------------|-------------|------|---------------------------------|
| Lech-Danube | Middle Holocene terrace | 3980-5040 | -- | Schielein et al. 2011 |
| Lech-Danube | Niederterrasse (NT) Lower terrace | 11230-11710 | -- | Schielein et al. 2011 |
| Colorado, TX | Youngest Deweyville | 1400-2000 | -- | Phillips 2006 |
| Rhine | Lower Terrace | 1100-1300 | -- | Kock et al. 2009 |
| Rio Negro | Rio Negro (III) Mariua´ archipelago | 1060-3650 | 90 | Latrubesse and Franzinelli 2005 |
| Umpqua | PHT Terrace, Elkton | 8630 | 100 | Personius 1993 |
| Sakarya River | T0 | 760 | 30 | Erturaç et al. 2019 |
| Sakarya River | T1 | 1000-1100 | -- | Erturaç et al. 2019 |
| Sakarya River | T2 | 9000 | 400 | Erturaç et al. 2019 |
| Sakarya River | T3 | 41100 | 1830 | Erturaç et al. 2019 |
| Erhjen River | C.P. | 7940-12054 | -- | Hsieh and Knuepfer 2001 |
| Erhjen River | HY | 5648-5935 | -- | Hsieh and Knuepfer 2001 |
| Erhjen River | HT | 6215-6306 | -- | Hsieh and Knuepfer 2001 |
| Erhjen River | HC | 9482-9535 | -- | Hsieh and Knuepfer 2001 |
| Erhjen River | KT1 | 1510-5984 | -- | Hsieh and Knuepfer 2001 |
| Erhjen River | KT2 | 1194-1294 | -- | Hsieh and Knuepfer 2001 |
| (Lower) Sabine | Deweyville Terraces | 4000-9000 | -- | Phillips and Slattery 2007 |

Table S3. Examples list of river terraces formed during the Holocene.

References

Anderson, J. B., Wallace, D. J., Simms, A. R., Rodriguez, A. B., Weight, R. W. R., & Taha, Z. P., (2016) Recycling sediments between source and sink during a eustatic cycle: Systems of late Quaternary northwestern Gulf of Mexico Basin. *Earth-Science Rev.*, 111–138. <https://doi.org/10.1016/j.earscirev.2015.10.014>.

Castelltort, S., & Van Den Driessche, J. (2003) How plausible are high-frequency sediment supply-driven cycles in the stratigraphic record? *Sedimentary Geology*, 157, 3–13. [https://doi.org/10.1016/S0037-0738\(03\)00066-6](https://doi.org/10.1016/S0037-0738(03)00066-6).

Erturaç, M.K., Şahiner, E., Zabcı, C., Okur, H., Polymeris, G.S., Meriç, N., & İkiel, C.(2019) Fluvial response to rising levels of the Black Sea and to climate changes during the Holocene: Luminescence geochronology of the Sakarya terraces. *The Holocene*, 29, 941–952, <https://doi.org/10.1177/0959683619831428>.

Hölz, S., (2021). Curve Intersect 2
(<https://www.mathworks.com/matlabcentral/fileexchange/8908-curve-intersect-2>),
MATLAB Central File Exchange.

Hsieh, M.-L., & Knuepfer, P.L.K. (2001) Middle–late Holocene river terraces in the Erhjen River Basin, southwestern Taiwan—implications of river response to climate change and active tectonic uplift. *Geomorphology*, 38, 337–372, [https://doi.org/10.1016/s0169-555x\(00\)00105-7](https://doi.org/10.1016/s0169-555x(00)00105-7).

Kock, S., Huggenberger, P., Preusser, F., Rentzel, P., & Wetzel, A.(2009) Formation and evolution of the Lower Terrace of the Rhine River in the area of Basel. *Swiss Journal of Geosciences*, 102, 307–321, <https://doi.org/10.1007/s00015-009-1325-1>.

Latrubesse, E.M., & Franzinelli, E. (2005) The late Quaternary evolution of the Negro River, Amazon, Brazil: Implications for island and floodplain formation in large anabranching tropical systems. *Geomorphology*,70, 372–397, <https://doi.org/10.1016/j.geomorph.2005.02.014>.

Li, Q., Yu, L., & Straub, K.M. (2016) Storage thresholds for relative sea-level signals in the stratigraphic record. *Geology*, 44, 179–182. <https://doi.org/10.1130/G37484.1>.

Personius, S.F. (1993) Age and origin of the fluvial terraces in the central Coast Range, western Oregon. *U.S. Geological Survey Bulletin*, 2038, <https://doi.org/10.3133/b2038>.

Phillips, J.D., (2006). *Geomorphic Context, Constraints, and Change in the lower Brazos and Navasota Rivers, Texas*. Retrieved from https://www.twdb.texas.gov/publications/reports/contracted_reports/doc/2005483564_Phillips.pdf

Phillips, J.D., & Slattery, M.C., (2007). *Geomorphic Processes, Controls, and Transition Zones in the Lower Sabine River*. Retrieved from https://www.twdb.texas.gov/publications/reports/contracted_reports/doc/0600010595_Sabine.pdf

Schielein, P., Schellmann, G., & Lomax, J. (2011) Stratigraphy of Late Quaternary fluvial terraces at the confluence of the Lech and Danube valleys. *E&G Quaternary Science Journal*, 60, 414–424, <https://doi.org/10.3285/eg.60.4.02>.

Stinchcomb, G.E., Driese, S.G., Nordt, L.C., & Allen, P.M. (2012) A mid to late Holocene history of floodplain and terrace reworking along the middle Delaware River valley, USA. *Geomorphology*, 169-170, 123–141, <https://doi.org/10.1016/j.geomorph.2012.04.018>.

Sylvester, Z., Deptuck, M., Prather, B., Pirmez, C., & O'Byrne, C. (2012) Seismic Stratigraphy of a Shelf-Edge Delta and Linked Submarine Channels in the Northeastern Gulf of Mexico: Application of the Principles of Seismic Geomorphology to Continental-Slope and Base-of-Slope Systems. *Case Studies from Seafloor and Near-Seafloor Analogues*, 31–59, <https://doi.org/10.2110/pec.12.99.0031>.

Yu, L., Li, Q., & Straub, K.M. (2017) Scaling the response of deltas to relative-sea-level cycles by autogenic space and time scales: A laboratory study. *Journal of sedimentary research*, 87, 817–837. <https://doi.org/10.2110/jsr.2017.46>.